CrystEngComm

Accepted Manuscript

ROYAL SOCIETY OF CHEMISTRY

www.rsc.org/crystengcomm

Morphology control and piezoelectric response of $Na_{0.5}Bi_{0.5}TiO_3$ synthesized via hydrothermal method

Xuefan Zhou, Chao Jiang, Chao Chen, Hang Luo, Kechao Zhou, Dou Zhang *

State key Laboratory of Powder Metallurgy, Central South University, Changsha, Hunan 410083, China

Abstract: In this study, lead-free sodium bismuth titanate ($Na_{0.5}Bi_{0.5}TiO_3$, NBT) was synthesized using hydrothermal method with processing temperatures of 100-180°C and NaOH concentrations of 2-14 M. NBT spherical agglomerates of primary nanocubes, NBT nanowires and NBT microcubes were obtained and their morphologies exhibited strong correlation with synthesis conditions. NBT nanowires with high aspect ratio were proven to be single-crystalline with [110] growth direction by high-resolution TEM analysis. The in-situ transformation process and dissolution-recrystallization mechanism were successfully used to explain the formation of different NBT morphology. Domain structures and piezoelectric characteristics were systematically studied for NBT by piezoresponse force microscopy (PFM). Clear ferroelectric domain structures and obvious polarization switching behaviors were observed in all types of NBT. The NBT microcubes possessed larger piezoresponse compared with NBT spherical agglomerates and nanowires.

Key words: $Na_{0.5}Bi_{0.5}TiO_3$, morphology control, piezoresponse, lead free, hydrothermal method

* Corresponding author.Tel./fax:+86 731 88877196

E-mail address: dzhang@csu.edu.cn (D. Zhang)

1 Introduction

In recent years, miniaturization and nanoengineering of piezoelectric devices have attracted great interest [1-3]. It is crucial to utilize micro-/nano- scaled and low-dimensional piezoelectric materials with designed and controllable morphology for applications in advanced sensors, transducers and energy harvesting devices [4-7]. Anisotropic plate-like templates have been successfully employed in grain orientated process, i.e. templated grain growth (TGG), which led to much improved properties of textured piezoelectric ceramics [8-9]. Piezoelectric nanowires have extensively been used in energy-harvesting devices and nano-electromechanical systems owing to their capability to effectively collect irregular tiny mechanical energy of different amplitudes and frequencies in environment [10-11]. Piezoelectric microspheres were often used to prepare 0-3 type piezoelectric composites [12]. Single-crystalline piezoelectric microcubes were used to form aligned microcrystal arrays and then were filled with matrixes to produce monolayer or multilayer textured composites [13-14]. In this regard, dimension, size and morphology control of piezoelectric materials is an effective route to develop novel piezoelectric devices and achieve better performance.

Traditional lead-based piezoelectric ceramics such as Pb(Zr, Ti)O_3 (PZT) and $(1–x)Pb(Mg_{1/3}Nb_{2/3})O_3–xPbTiO_3$ possess superior piezoelectric properties [15-16], but the toxicity of lead oxide and the high volatility of Pb during processing limits their applications. Among the numerous lead free piezoelectric materials, sodium bismuth titanate ($Na_{0.5}Bi_{0.5}TiO_3$, NBT) is considered to be a prominent candidate to replace lead-based piezoelectric ceramics [17]. NBT is a perovskite type ferroelectric with high Curie temperature of about 320 ℃. It exhibits rhombohedral structure at room temperature and shows a relatively strong remnant polarization of 38 μC/cm^2 [18-19].

Recently, hydrothermal synthesis of NBT has drawn attention owing to the outstanding morphology control, the low temperature process, homogeneity at the molecular level, high degree of crystallinity, high purity and narrow particle size distribution[20-21]. It was reported that the morphology of NBT evolved from nanoplates to cubes at 200 ℃ with NaOH concentration increasing from 8 to 18 M and finally became nanowires with prolonging the holding time to 60 h. The formation mechanisms were proposed to be in-situ transformation process, dissolution-recrystallization mechanism and oriented attachment mechanism, respectively [22]. Besides, monosized NBT spherical particles were obtained at

200 ℃ with a relatively low alkalinity [23]. Single-crystalline NBT nanowires can also be synthesized by a sol-gel hydrothermal technique[24].

Based on previous work, we aimed to achieve the morphology control of NBT under milder hydrothermal conditions and study their piezoelectric responses to investigate their suitability to applications. In this work, the influences of processing temperature and NaOH concentration on the synthesis of NBT were investigated systematically. NBT spherical agglomerates were obtained at a low temperature of 150 ℃. Single-crystalline NBT nanowires and microcubes were obtained at 170 ℃ for 48 h with NaOH concentration of 10 M and 14 M, respectively. The in-situ transformation process and dissolution-recrystallization mechanism were successfully used to explain the formation of NBT spherical agglomerates, nanowires and microcubes. Moreover, the domain structures and local piezoresponses were investigated in detail by piezoresponse force microscopy (PFM).

2 Material and methods

2.1 Synthesis of the NBT

Bismuth nitrate pentahydrate ($Bi(NO_3)_3{\cdot}5H_2O$, Sinopharm, China, ≥99.9%), sodium nitrate ($NaNO_3$, Sinopharm, China, ≥99.0%), tetrabutyl titanate ($Ti(OC_4H_9)_4$, Sinopharm, China, ≥98.0%), acetic acid (CH_3COOH, Sinopharm, China, ≥99.5%) and ethanol (CH_3CH_2OH, Sinopharm, China, ≥99.7%) were used as raw materials. Sodium hydroxide (NaOH, Sinopharm, China, ≥96.0%) was used as mineralizer. Firstly, 0.005 mol $Bi(NO_3)_3{\cdot}5H_2O$, 0.01 mol $NaNO_3$ and 0.005 mol $Ti(OC_4H_9)_4$ were dissolved in 7.5 ml CH_3COOH, 2.5 ml distilled water and 10 ml CH_3CH_2OH respectively. Secondly, the $Bi(NO_3)_3{\cdot}5H_2O$ and $NaNO_3$ solutions were added into $Ti(OC_4H_9)_4$ solution, which subsequently formed a suspension with the addition of NaOH solution (2-14M). The suspension was continually stirring for 1 h. Finally, the hydrothermal reactions were carried out at processing temperature of 100-180℃ under auto-generated pressure for 48 h in a 100 ml Teflon-lined autoclave with a filling capacity of 50%. The autoclave was cooled down to room temperature naturally after the reaction completed. The products were washed by distilled water several times and dried at 80 ℃ in a oven.

2.2 Characterization of the NBT

The crystalline phases of the products were tested by X-ray diffraction (XRD, D/max 2550, Japan) with Cu-Kα radiation (λ=1.5406 Å) at room temperature. The diffraction data were recorded in the 2θ range of 20 - 80 degree with a scan step of 0.02^{o}. Rietveld refinements were carried out using Jade 6.5 software package (Materials Data, Inc.). The size and morphology of the products were observed using a scanning electron microscope (SEM, Nova NanoSEM230, USA). The compositional analysis was carried out by energy dispersive spectrometer (EDS). High-resolution transmission electron microscopy (HRTEM) images of the synthesized NBT were taken with a JEM-2100F transmission electron microscope, using an accelerating voltage of 200 kV.

The piezoelectric characteristics of NBT were investigated by the piezoresponse force microscopy (PFM) contact mode of an atomic force microscope (NanoManTM VS) with a conductive Pt/Ir-coated Si cantilever (SCM-PIT), which has a spring constant of 2.8 N/m and a free resonance frequency of 75 kHz. NBT particles were dispersed on Pt-electroded Si wafers. An alternating current (AC) voltage with amplitude of 8 V and frequency of 41 kHz, away from the contact resonance, was applied between the Pt-coated tip and Pt electrode to visualize the domain structures. During the switching test, the tip was fixed on the particle surface and a direct current (DC) voltage from -10 to 10V was applied superimposed on an AC modulation voltage. The piezoresponse amplitude and the phase difference were concurrently acquired.

3 Results and discussion

3.1 Phase evaluation and morphology

Fig. 1a shows the observed XRD patterns of the products hydrothermally synthesized for 48 h with NaOH concentration of 10 M at the processing temperatures ranging from 100 ℃ to 180 ℃. At the lowest processing temperature of 100 ℃, the observed XRD pattern of synthesized products showed three obvious diffraction peaks indexed with the pyrochlore phase of $Bi_{12}TiO_{20}$ (PDF card NO.34-0097) and other weak diffraction peaks were indexed to monoclinic NBT. $Bi_{12}TiO_{20}$ was a mesophase before the formation of NBT. With increasing the hydrothermal temperature to the range of 120 - 170 ℃, the observed XRD patterns showed that

phase-pure NBT was obtained which corresponding to monoclinic NBT (PDF card NO.46-0001). However, when the processing temperature increased to 180 °C, an obvious additional peak appeared at 30° and was indexed to the impurity phase of $Bi_4Ti_3O_{12}$ (PDF card NO.35-0795). These results showed phase-pure monoclinic NBT were obtained at the processing temperatures of 120 - 170 °C. The Rietveld refinements of X-ray diffraction data at 120 °C to 170 °C were carried out by Jade 6.5 program and the magnified view of (101) peak is shown in Fig. 1b. The black lines in Fig. 1b are corresponding calculated XRD patterns. The refinement parameter *R* for all samples is less than 10 %. Fig. 1c shows the relationship between the full width at half maximum (FWHM) of (101) peak obtained from calculated XRD patterns and processing temperatures. The (101) peak became stronger and the FWHM decreased with the increase of hydrothermal temperature, indicating that the crystallization of NBT was improved at higher processing temperature and the best crystallinity was obtained at 170 °C.

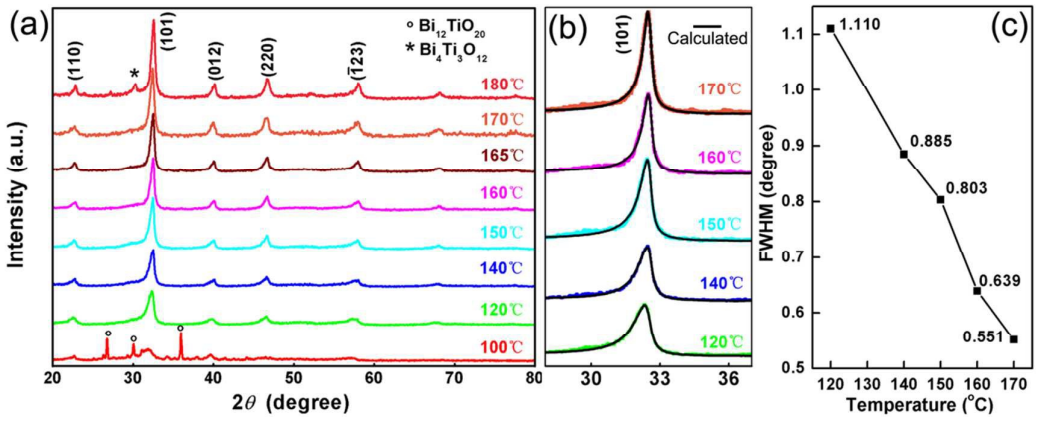

Fig. 1 (a) The observed XRD patterns of the products hydrothermally synthesized for 48 h with NaOH concentration of 10 M and processing temperature ranging from 100 °C to 180 °C. (b) The observed and calculated XRD partterns of (101) peak at 120 °C to 170 °C. (c) The relationship between the FWHM of (101) peak and processing temperature ranging from 120 °C to 170 °C.

Fig. 2 shows the sizes and morphologies of NBT hydrothermally synthesized for 48 h with NaOH concentration of 10 M at the processing temperatures ranging from 120 °C to 170 °C. When the processing temperature was 120 °C, the synthesized

products were relatively uniform and exhibited spherical agglomerates with diameters of about 1.30 μm, which, however, were consisted of smaller primary nanoparticles and were not monodispersed as shown in Fig. 2a and Fig. 2b. When the processing temperature increased to 140 °C (Fig. 2c and Fig. 2d) and 150 °C (Fig. 2e and Fig. 2f), the synthesized products became monodispersed spherical agglomerates with the diameters of about 1.40 μm and 1.50 μm, respectively, which were slightly bigger than the former. When the processing temperature increased to 160 °C (Fig. 2g and Fig. 2h), it is obvious that a handful of nanowires appeared in synthesized products and the aggregated spherical particles were agglomerated by smaller nanocubes. The diameter of the spherical agglomerates was about 1.20 μm which was smaller than the spherical agglomerates synthesized at 150 °C. Based on the above results, with the processing temperature increasing from 120 °C to 160 °C, spherical agglomerates generally grew bigger until a handful of nanowires appeared at 160 °C. The amount of nanocubes in primary nanoparticles increased. Also, the edge and surface of nanocubes became more distinct and smoother, respectively. When the processing temperature increased to 170 °C (Fig. 2i and Fig. 2j), it can be seen that a mass of nanowires with diameters of about 100 nm and lengths of about 20 μm were formed accompanied by much less amount of spherical agglomerates. The NBT nanowires were flexible and had flat and smooth surfaces.

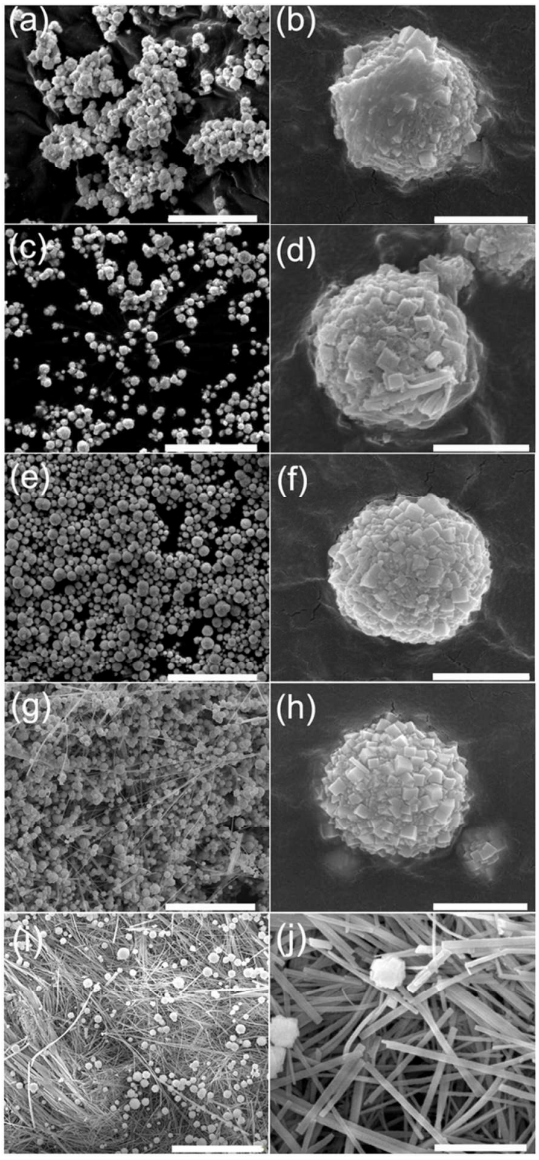

Fig. 2 The SEM images of NBT hydrothermally synthesized for 48 h with NaOH concentration of 10 M and processing temperatures of (a) 120 °C, (c) 140 °C, (e) 150 °C, (g) 160 °C and (i) 170 °C respectively. (b), (d), (f), (h) and (j) are SEM images with higher magnification of (a), (c), (e), (g) and (i) respectively. Scale bars for (a), (c), (e), (g) and (i) are 10 μm. Scale bars for (b), (d), (f), (h) and (j) are 1 μm.

According to the XRD results shown in Fig. 1 and the SEM results shown in Fig. 2, the processing temperature of 170 °C was favorable for the synthesis of NBT with high crystallinity and the formation of NBT nanowires. Besides the processing temperature, the concentration of NaOH (OH^-) also affects the crystallinity and

morphology of the NBT significantly. Fig. 3a shows the observed XRD patterns of the products hydrothermally synthesized at 170 °C for 48 h with NaOH concentration ranging from 2 M to 14 M. The observed XRD patterns of synthesized products showed that phase-pure NBT was obtained when NaOH concentration ranged from 6 M to 14 M. At low NaOH concentration of 2 M, the synthesized products were yellowish and there existed pyrochlore phase $Bi_{12}TiO_{20}$. The weak corresponding diffraction peaks showed the products synthesized under this condition were amorphous. At 4 M, NBT phase appeared but the corresponding characteristic diffraction peaks were also weak with the existence of the impurity. When NaOH concentration was increased to 6 M, the characteristic diffraction peaks of pure NBT phase with perovskite structure were obtained. Fig. 3b shows the observed and calculated XRD partterns of (101) peak at 6 M to 14 M. The refinement parameter *R* for all samples is less than 10 %. Fig. 3c shows the relationship between the FWHM of (101) peak obtained from calculated XRD patterns and NaOH concentrations. NaOH offered the alkalinity needed by crystallization process. With NaOH concentration increasing from 6 M to 14 M, it was found that the intensity of NBT diffraction peaks increased according to Fig .3a and the FWHM of (101) peak decreased according to Fig .3c which revealed that well crystallized NBT were synthesized facilely in stronger alkaline solution.

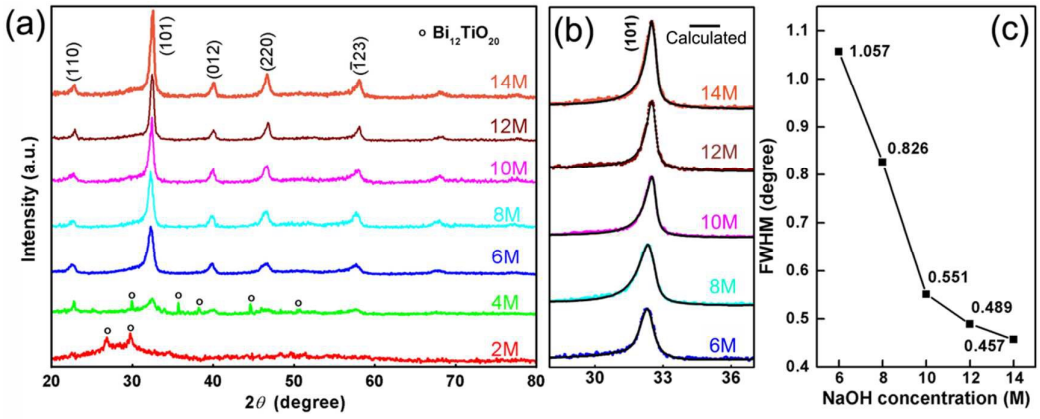

Fig. 3 (a) The XRD patterns of the products hydrothermally synthesized at 170 °C for 48 h with NaOH concentration ranging from 2 M to 14 M. (b) The observed and calculated XRD partterns of (101) peak at 6 M to 14 M. (c) The relationship between the FWHM of (101) peak and NaOH concentrations.

Fig. 4 shows the sizes and morphologies of NBT hydrothermally synthesized at 170 °C for 48 h with NaOH concentration ranging from 6 M to 14 M. At 6 M, the spherical agglomerates with diameters of about 0.5 μm and some amorphous materials were obtained, as shown in Fig. 4a. The spherical agglomerates were consisted of spherical primary nanoparticles with the average size of 10-20 nm. At 7 M, the synthesized products were only spherical agglomerates consisted of regular nanocubes with the size of 30-70 nm. The nanocubes possessed clear edges and smooth surfaces as shown in Fig. 4b. At 8 M, some nanowires appeared together with spherical agglomerates as shown in Fig. 4c. The amount of nanowires in synthesized products also increased with increasing NaOH concentration to 9 M as shown in Fig. 4d. At 10 M, high aspect ratio nanowires became dominant in synthesized products as described in Fig. 2, which also were shown in Fig. 4e. At 12 M, some submicron cubes with the size of 100-200 nm and some plates formed irregular aggregated particles, as shown in Fig. 4f. At 13 M, it can be seen that the cubes became bigger and zigzag edges appeared on the surface. The cubes were embedded with each other as shown in Fig. 4g. When NaOH concentration was 14 M, NBT became regular cubic and showed smooth surfaces and clear edges with about 1 μm edge length, as shown in Fig. 4h.

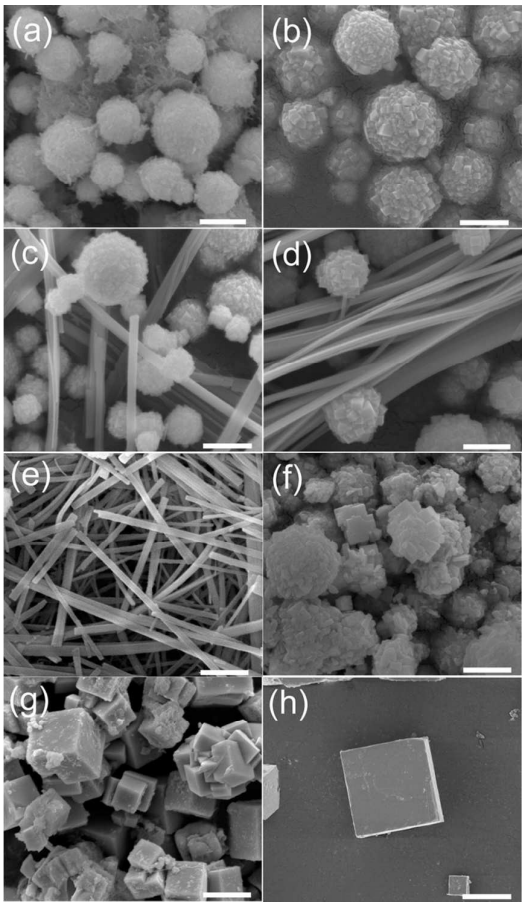

Fig. 4 The SEM images of NBT particles hydrothermally synthesized at 170 ℃ for 48 h with NaOH concentrations of (a) 6 M, (b) 7 M, (c) 8 M, (d) 9 M, (e) 10 M, (f) 12 M, (g) 13 M and (h) 14 M respectively. Scale bars are 0.5 μm.

These results demonstrated the morphology evolution of NBT was clear and significant during the hydrothermal process. It can be revealed that more NBT nuclei were formed with increasing the processing temperature and NaOH concentration. Stronger alkaline solution and higher processing temperature facilitated the individual growth of NBT nuclei. It's obvious that reaction parameters such as the concentration of mineralizer and the processing temperature have great impacts on the properties of synthesized products in hydrothermal method [25]. Three specific morphologic NBT were obtained, including spherical agglomerates of nanocubes synthesized at 150 ℃ for 48 h with NaOH concentration of 10 M, nanowires synthesized at 170 ℃ for 48 h with NaOH concentration of 10 M and microcubes synthesized at 170 ℃ for 48 h with NaOH concentration of 14 M.

3.2 Formation mechanism

The formation mechanisms of NBT with different morphology include in-situ transformation and dissolution-recrystallization as shown in Fig. 5. They have been applied successfully to explain the hydrothermal synthesis of many perovskite materials [22, 24, 26]. In the study of Lu. *et. al* [22], the two mechanisms were proposed to explain the formation of NBT nanoplates and cubes synthesized from TiO_2 and $Bi(NO_3)_3{\cdot}5H_2O$. In this work, $Ti(OC_4H_9)_4$ and $Bi(NO_3)_3{\cdot}5H_2O$ were hydrolyzed to $TiO_2{\cdot}nH_2O$ and $Bi_2O_3{\cdot}nH_2O$ and subsequently dissolved into Ti^{4+} complex ions, $Ti(OH)_x^{(4-x)}$ and Bi^{3+} respectively, as shown in Fig. 5a. The dissolution rate of $Bi_2O_3{\cdot}nH_2O$ was much higher than that of $TiO_2{\cdot}nH_2O$, resulting in a sluggish dissolution - crystallization process [22]. When the processing temperature and NaOH concentration were relatively low, the pre-dissolved Bi^{3+} and Na^+ were absorbed onto the surfaces of $TiO_2{\cdot}nH_2O$ particles and then topotactically changed into more stable NBT via in situ transformation as shown in Fig. 5b. When the processing temperature and NaOH concentration were relatively high, aqueous metal species formed by dissolution of the precursors recrystallized from the supersaturated solution [22]. In the heterogeneous nucleation process, a few $Ti(OH)_x^{(4-x)}$ and abundant pre-dissolved Bi^{3+} and Na^+ were absorbed onto the surface of $TiO_2{\cdot}nH_2O$ for reducing the surface free energy. NBT crystal nuclei were formed on the surface of $TiO_2{\cdot}nH_2O$ particles when the density of precursors achieved the critical nucleation density and NBT spherical agglomerate were obtained as shown in Fig. 5c. In the homogeneous nucleation process, dissolved Bi^{3+}, $Ti(OH)_x^{(4-x)}$ and Na^+ were homogeneously dispersed in the solution. NBT crystal nucleuses were formed in the solution directly. NBT nanowires were directly precipitated from the homogeneous solution via chemical reaction [24], as shown in Fig. 5d. NBT microcubes were obtained as shown in Fig. 5e, with the classical crystal growth mode including a short nucleation period and an Ostwald ripening process [27]. The increase of NaOH concentration and processing temperature is favourable for the formation of the uniform NBT cubes in the hydrothermal reaction.

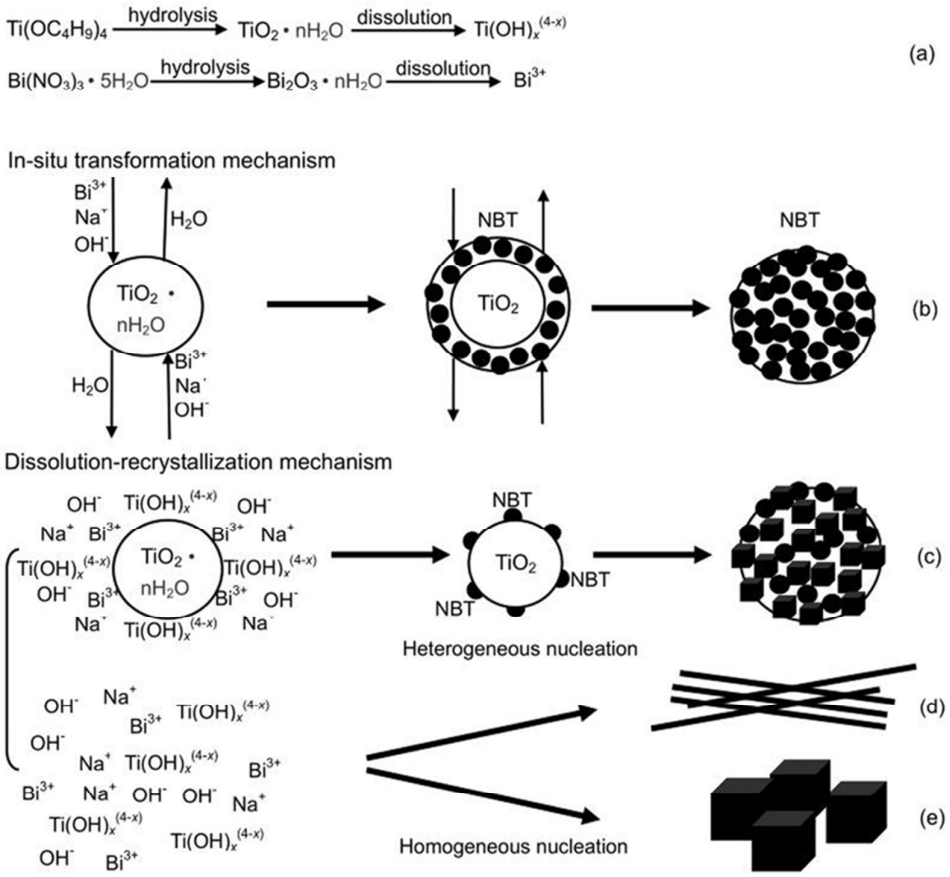

Fig. 5 Schematic illustration of the formation mechanisms. (a) Hydrolysis and dissolution process of titanium precursor and bismuth precursor. (b) In-situ transformation process. (c) Heterogeneous nucleation process with dissolution-recrystallization mechanism. (d) (e) Homogeneous nucleation process with dissolution-recrystallization mechanism.

3.3EDS analysis and HRTEM observation of NBT

Fig. 6 shows the EDS analysis of synthesized NBT spherical agglomerates, nanowires and microcubes. The insets in Fig. 6 are corresponding detailed compositions of NBT. The analysis results proved that all three specific morphologic NBT were composed of Bi, Na, Ti, and O with the atomic ratio of approximately 1 : 1 : 2 : 6, which was consistent with the stoichiometric ratio of NBT. The existence of Au and C elements was due to their employment as conducting mediums for SEM observation.

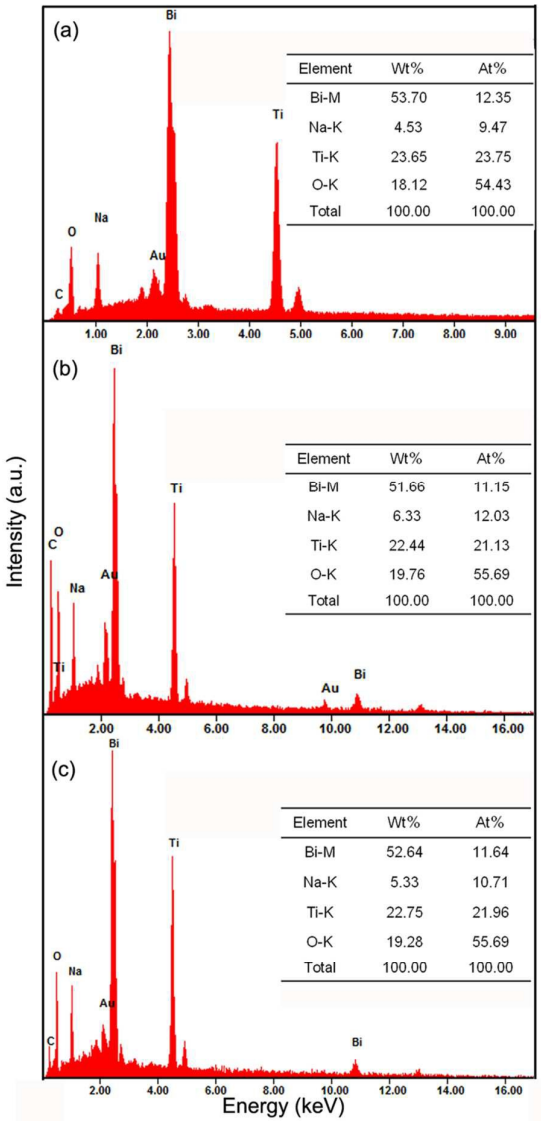

Fig. 6 EDS analysis of NBT spherical agglomerates (a), nanowires (b) and microcubes (c). Insets: the corresponding detailed compositions of NBT.

Fig. 7a, Fig. 7c and Fig. 7e show the TEM micrographs of synthesized NBT spherical agglomerates, nanowires and microcubes, respectively. The corresponding HRTEM images and fast Fourier transform (FFT) patterns are shown in Fig. 7b, Fig. 7d and Fig. 7f, respectively. The NBT spherical agglomerates were agglomerated by primary nanocubes. The HRTEM image of the nanocube showed clear lattice fringes and the parallel lattice spacing were about 0.388 nm and 0.274 nm corresponding to (110) and (-102) planes of monoclinic NBT, respectively, as shown in Fig. 7b. The NBT nanowire possessed smooth surface with diameter of about 100nm. The clear lattice fringes shown in Fig. 7d illustrated that the as-synthesized nanowires were single-crystalline. The parallel lattice spacing were about 0.193 nm and 0.224 nm corresponding to (220) and (012) planes of monoclinic NBT respectively, which revealed that the nanowires grew in the [110] direction. The FFT pattern shown in the inset further confirmed the single-crystalline nature of the nanowire and the formation of monoclinic NBT. The NBT microcubes possessed smooth surface and well-defined edges. The lattice fringes shown in Fig. 7f illustrated that the NBT microcubes were single-crystalline. The parallel lattice spacing were about 0.387 nm and 0.276 nm corresponding to (110) and (-121) planes of monoclinic NBT, respectively.

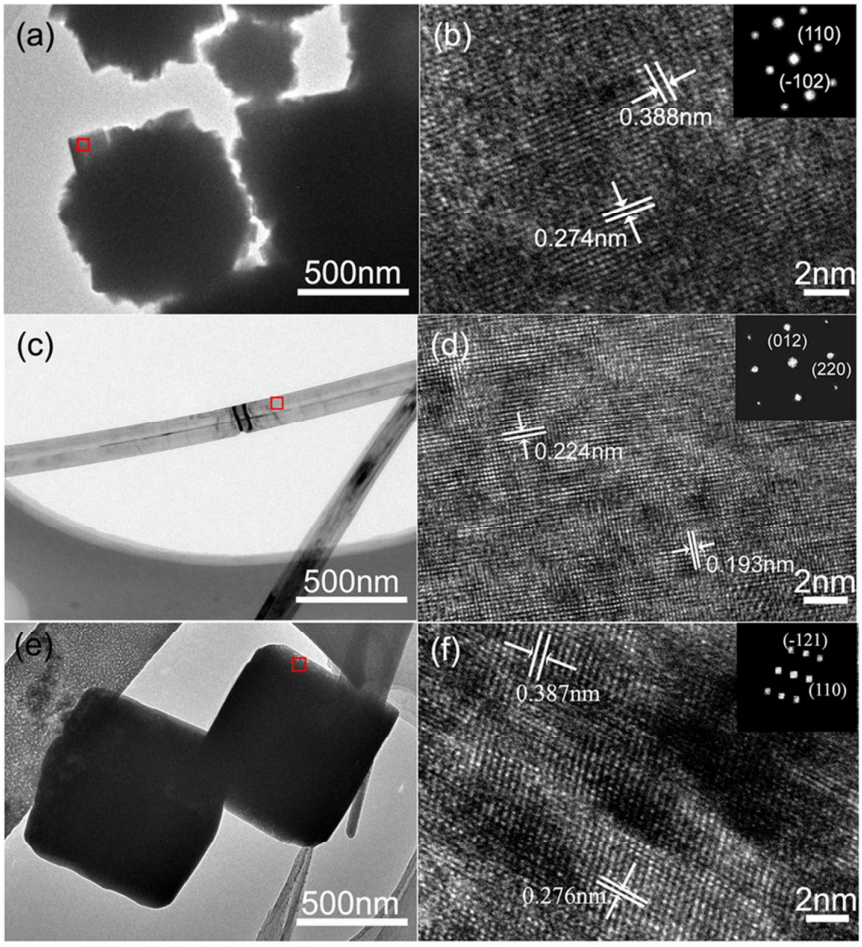

Fig. 7 The TEM micrographs and HRTEM images of (a) (b) NBT spherical agglomerates, (c) (d) nanowires and (e) (f) microcubes. Insets: The corresponding FFT patterns of NBT.

3.4 Piezoelectric characteristics

Contact mode PFM was applied to reveal the out-of-plane piezoresponse of the hydrothermally synthesized NBT. Figure 8 shows the topographic images and domain structures of NBT spherical agglomerates, nanowires and microcubes. The topographic images shown in Fig .8a presents that the NBT spherical agglomerate was agglomerated by smaller NBT nanoparticles. PFM amplitude image and phase image of the NBT spherical agglomerate both exhibits partly blurry ferroelectric domain structures as shown in Fig .8b and Fig .8c, respectively. The brightness in the amplitude image shows the strength of piezoresponse, whereas the contrast in the phase image was determined by polarization orientations of detected regions [28].

PFM domain contrasts shown in Fig. 8c indicated the presence of polarized nanoregions with different polarization orientations. By comparing the topographic image and phase image of the NBT spherical agglomerate, it is found that adjacent grains may possess the same polarization direction.

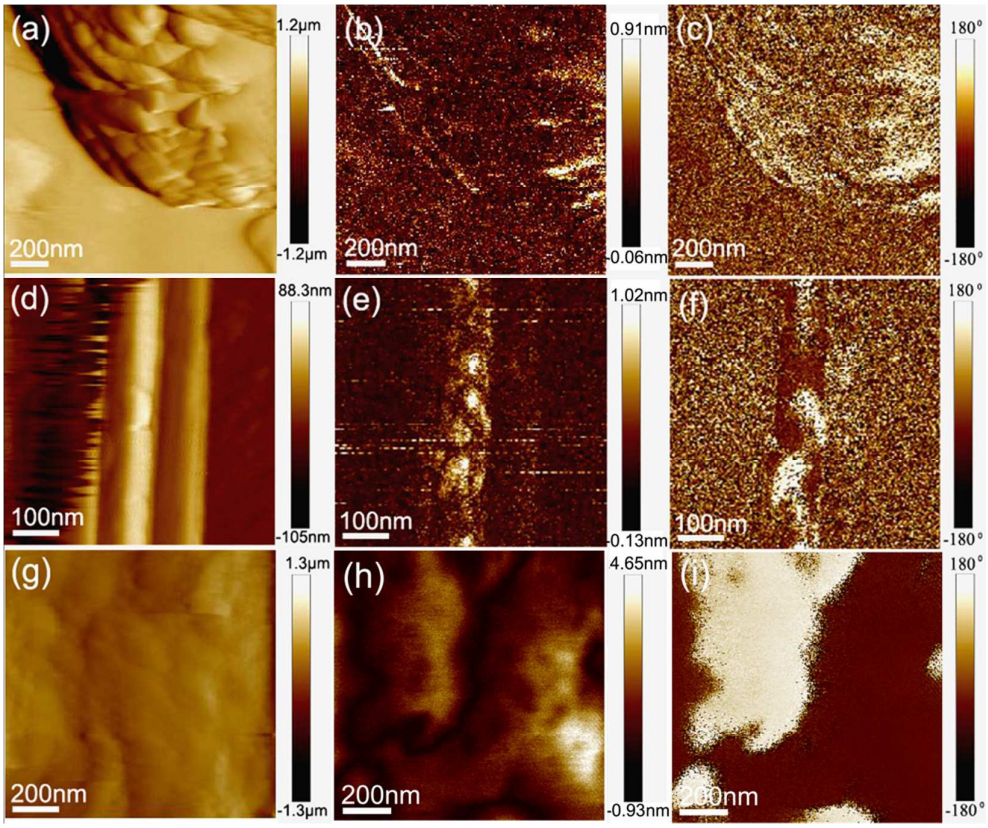

Figure 8 The topographic images, PFM amplitude images and PFM phase images of NBT, respectively. (a) (b) (c) NBT spherical agglomerate, (d) (e) (f) NBT nanowire, (g) (h) (i) NBT microcube.

Fig .8d presents the topographic image of the NBT nanowire, showing a smooth surface. Within the individual NBT nanowire, strong and clear contrasts were observed in the amplitude image and phase image, as shown in Fig .8e and Fig .8f , which indicated the presence of polarized nanoregions in the NBT nanowire. These domains were grainy and possessed 180^0 phase difference contrast. Meanwhile, It revealed the NBT nanowire has a multidomain structure. Fig .8g shows the topographic image of one face of the NBT microcube. The amplitude image and

phase image also presented strong and clear PFM domain contrast, indicating the NBT microcube also has a multidomain structure. The difference was the average size of ferroelectric domains in the single crystalline NBT microcube was about 300-500nm which was much larger than that in the NBT spherical agglomerate and single crystalline nanowire (50-100nm). Besides, the maximum amplitudes in the NBT spherical agglomerate and nanowire were 0.91nm and 1.02nm, respectively which was 4.65nm in the NBT microcube.

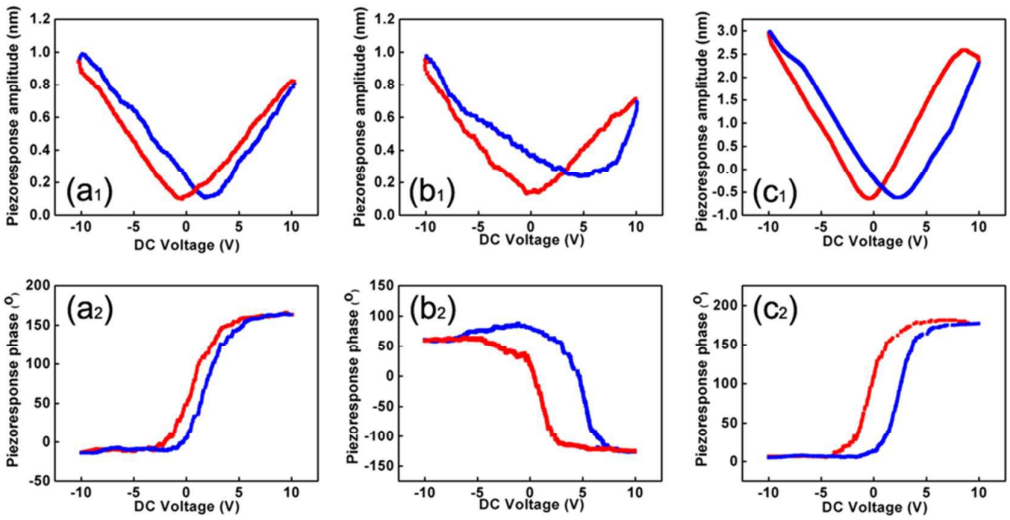

Fig. 9 The amplitude-voltage butterfly loops (subscript 1) and phase-voltage hysteresis loops (subscript 2) of (a) NBT spherical agglomerate, (b) nanowire and (c) microcube.

For studying the polarization switching behaviors, the local piezoresponse was examined by applying a direct current (DC) voltage from -10 to 10V between the Pt-coated tip and Pt electrode. For all the NBT with different morphologies, the classic amplitude-voltage butterfly loops and phase-voltage hysteresis loops were observed as shown in Fig. 9 which confirmed the local piezoelectricity of NBT. Fig. 9a, Fig. 9b and Fig. 9c show the amplitude-voltage butterfly loops and phase switching of NBT spherical agglomerate, nanowire and microcube, respectively. For all types of NBT, phase reversal was observed in the piezoresponse phase-voltage hysteresis loops when a coercive voltage was exceed. The phase contrast was about 180^0 indicating the existence of 180^0 domains in the NBT and a clear polarization switching process [27]. It can be also found that all the amplitude-voltage butterfly loops were shifted toward

a positive volatage, reflecting the presence of an internal electric field [29]. The maximum electrically-induced displacements of NBT spherical agglomerate, nanowire and microcube were measured to be approximately 1nm, 1nm, and 3nm respectively. The amplitude-voltage butterfly loop of NBT microcube was better defined and more opened than that of NBT spherical agglomerate and nanowire. The reason of these differences was supposed to be the effect of grain size on piezoresponse. It has been reported that the reduction of grain size to the nanoscale results in the disappearance of ferroelastic domains and causes the reduction of the extrinsic contributions to piezoelectricity [30]. It should be underlined that the local piezoresponse was measured inside an individual grain. On this basis, although the diameter of NBT spherical agglomerate was about 1.50 μm, the AFM tip actually only fixed on the surface of a primary nanoparticle.

On the whole, the three specific morphologic NBT all presented characteristic piezoresponse with ferroelectric domain structures and obvious polarization switching behaviors. In contrast, single-crystalline NBT microcube showed relatively larger ferroelectric domain and piezoresponse than NBT spherical agglomerate and single-crystalline NBT nanowire.

4 Conclusion

In summary, the morphology control of NBT was achieved and obtain the piezoelectric characteristics of NBT with different morphology. The morphology evolved from spherical agglomerates to nanowires and finally were microcubes at 170 ℃ for 48 h when the initial NaOH concentration ranged from 2 M to 14 M. Monodispersed and monosized NBT spherical agglomerates about 1.5 μm in diameter with good crystallinity were obtained for 48 h with NaOH concentration of 10 M and the processing temperature of 150 ℃. The NBT nanowires with diameters of about 100 nm and lengths of 20 μm were obtained at 170 ℃ for 48 h when NaOH concentration was 10 M. The single-crystalline NBT nanowires grew in the [110] direction. The single-crystalline NBT microcubes with edge lengths of about 1 μm were obtained at 170 ℃ for 48 h when NaOH concentration was 14 M. In-situ transformation mechanism and dissolution-recrystallization mechanism were used to explain the formation of various morphological NBT. The PFM investigations confirmed the piezoelectricity of NBT spherical agglomerates, nanowires and microcubes. The NBT microcubes revealed larger ferroelectric domain and local piezoresponse compared with NBT spherical agglomerates and nanowires. They can have promising applications in high-performance and miniaturized piezoelectric devices.

Acknowledgment

This work was financially supported by Hunan Nonferrous Research Funding (No: YSZN2013CL05), Ph.D. Programs Foundation of Ministry of Education of China (NO. 20110162110044), Hunan Doctoral Research Innovation Project (No: CX2014B055), and Graduate student research innovation project in Hunan Province (NO. 150140011).

Reference

[1] S. Xu, B. J. Hansen, Z. L. Wang, Nat. Commun., 1 (7) (2010) 1-5.

[2] C. K. Jeong, I. Kim, K. I. Park, M. H. Oh, H. Paik, G. T. Hwang, K. No, Y. S. Nam, K. J. Lee, ACS Nano, 7 (12) (2013) 11016-11025.

[3] X. Chen, J. W. Li, G. T. Zhang, Y. Shi, Adv. Mater., 23 (34) (2011) 3965-3969.

[4] L. Gu, N. Y. Cui, L. Cheng, Q. Xu, S. Bai, M. M. Yuan, W. W. Wu, J. M. Liu, Y. Zhao, F. Ma, Y. Qin, Z. L. Wang, Nano Lett., 13 (1) (2013) 91-94.

[5] H. X. Tang, Y. R. Lin, H. A. Sodano, Adv. Energy Mater., 2 (4) (2012) 393-393.

[6] G. Xu, X. Yang, C. X. Hua, J. H. He, Z. H. Ren, W. J. Weng, P. Y. Du, G. Shen, G. R. Han, CrystEngComm, 14 (2012) 6783-6787.

[7] M. M. Kržmanc, I. Bračko, B. Budič, D. Suvorov, J. Am. Ceram. Soc., 96 (11) (2013) 3401-3409.

[8] C. Jiang, X. F. Zhou, K. C. Zhou, C. Chen, H. Luo, X. Yuan, D. Zhang, J. Eur. Ceram. Soc. (2015), doi:10.1016/j.jeurceramsoc.2015.12.025 .

[9] W. F. Bai, L. Y. Li, W. Li, B. Shen, J. W. Zhai, H. Chen, J. Alloys Compd., 603 (2014) 149-157.

[10] S. Bai, Q. Xu, L. Gu, F. Ma, Y. Qin, Z. L. Wang, Nano Energy, 1 (6) (2012) 789-795.

[11] C. David, J. F. Capsal, L. Laffont, E. Dantrasl, C. Lacabanne, J. Phys. D Appl. Phys., 45 (41) (2012) 1-7.

[12] M.T. Kamalia, H. M. Shodja, Int. J. Eng. Sci., 44 (10) (2006) 633-649.

[13] X. Y. Liu, E. F. McCandlish, L. E. McCandlish, K. Mikulka-Bolen, R. Ramesh, F. Cosandey, G. A. Rossetti, R. E. Riman, Langmuir, 21 (8) (2015) 3207-3212.

[14] Y. R. Lin, C. Andrews, H. A. Sodano, J. Appl. Phys., 108 (064108) (2010) 1-6.

[15] R. Xie, C. Liu, Y. Zhao, P. Jin, K. C. Zhou, D. Zhang, J. Eur. Ceram. Soc., 35 (7) (2015) 2051-2056.

[16] J. Jiang, H. J. Jung, S. G. Yoon, J. Alloys Compd., 509 (24) (2011) 6924-6929.

[17] C. Jiang, K. C. Zhou, X. F. Zhou, Z. Y. Li, D. Zhang, Ceram. Int., 41 (5) (2015) 6858-6862.

[18] G. A. Smolenskii, V. A. Isupo, A. I. Agranovskaya, N. N. Krainik, Sov. Phys. Solid State, 2 (11) (1961) 2651-2654.

[19] T. Takenaka, K. Sakata, Ferroelectrics, 95 (1) (1989) 153-156.

[20] Y. Deng, L. Liu, Y. Cheng, C. Nan, S. Zhao, Mater. Lett., 57 (11) (2003) 1675-1678.

[21] J. H. Lee, H. H. Nersisyan, H. H. Lee, C. W. Won, J. Mater. Sci., 39 (4) (2004) 1397-1401.

[22] R. Lu, J. Yuan, H. Shi, B. Li, W. Wang, D. Wang, M. Cao, CrystEngComm, 15 (19) (2013) 3984-3991.

[23] Y. Liu, Y. Lu, S. Dai, J. Alloys Compd., 484 (1-2) (2009) 801-805.

[24] J. B. Liu, H. Wang, Y. D. Hou, M. K. Zhu, H. Yan, M. Yoshimura, Nanotechnology, 15 (7) (2004) 777-780.

[25] J. F. Trelcat, S. d'Astorg, C. Courtois, P. Champagne, M. Rguiti, A. Leriche, J. Eur. Ceram. Soc., 31 (11) (2011) 1997-2004.

[26] J. Moon, J. A. Kerchner, H. Krarup, J. H. Adair, J. Mater. Res., 14 (2) (1999) 425-435.

[27] F. F. Guo, B. Yang, S. T. Zhang, D. Q. Liu, F. M. Wu, D. L. Wang, W. W. Cao, Appl. Surf. Sci., 283 (2013) 759-763.

[28] K. Prashanthi, T. Thundat, Scanning, 36 (2014) 224-230.

[29] M. Cernea, L. Trupina, C. Dragoi, B. S. Vasile, R. Trusca, J. Alloys Compd., 515 (2012) 166-170.

[30] N. Salazar, M. Algueró, H. Amorín, A. Castro, A. Gil, J. Ricote, J. Appl. Phys., 116 (124108) (2014) 1-8.